Submitted to Journal
of Chemical Physics

LBL-189
Preprint

REACTIONS OF MODULATED MOLECULAR BEAMS WITH PYROLYTIC GRAPHITE
I. Experimental Apparatus and Data Interpretation

R. Jones, D. R. Olander, W. Siekhaus, and J. A. Schwarz

October 1971

AEC Contract No. W-7405-eng-48

DISCLAIMER

REACTIONS OF MODULATED MOLECULAR BEAMS WITH PYROLYTIC GRAPHITE

I. Experimental Apparatus and Data Interpretation

by R. Jones, D. R. Olander, W. Siekhaus, and J. A. Schwarz

Inorganic Materials Research Division of the Lawrence Berkeley Laboratory and the Department of Nuclear Engineering, University of California, Berkeley, Calif. 94720

ABSTRACT

An apparatus for the study of gas-solid reactions which produce a gaseous reaction product is described. The reactant gas contacts the solid as a molecular beam travelling in vacuum. Gaseous reaction products are monitored by a mass spectrometer as they are emitted from the surface. The technique relies heavily upon the modulation of the molecular beam, which improves sensitivity by shifting the information from the very noisy zero frequency (dc) band to a narrow band ac mode which has considerably less noise. In addition, modulation of the reactant beam induces modulation at the same frequency in the reaction products and the phase difference between these two signals contains important kinetic information.

The method of comparing theoretical models of the surface processes with the phase and amplitude information provided by the experiment is described.

I. INTRODUCTION

The reactions between carbon and a variety of gases have been studied for decades. However, much of the early work has suffered from one or more of the following difficulties:

(1) Although carbon is available in crystalline forms such as natural graphite and diamond, most investigations (for reasons of practical interest and material fabricability) have employed poorly characterized amorphous carbons or isotropic graphites. When employed in the form of a powder, the true surface area upon which the heterogeneous reaction occurs is difficult to ascertain. The role of internal porosity in isotropic graphite complicates reaction analysis. Impurities in the sample may catalyze or poison a particular reaction. The exposed faces of amorphous carbon and polycrystalline graphite present a mixture of surfaces of different reactivity to the attacking gas.

(2) Carbon or graphite, owing to the refractory nature of the element, generally is reactive towards most common gases only above 500°C or so, and in reacting, produces a variety of product species. The product distribution of the primary heterogeneous reaction may be modified by secondary gas phase reactions or reactions with surfaces of the apparatus other than the carbon or graphite specimen.

(3) Most carbon-gas kinetic experiments have been conducted at "high" pressures; that is, under conditions where the mean free path of the molecules in the gas phase is less than the dimensions of the apparatus. At high temperatures, the heterogeneous reaction may be so rapid that the surface becomes starved of gaseous reactant. In such a situation, the measured reaction rate reflects substantial

contributions due to diffusion, either in the pores of the sample or in a hydrodynamic boundary layer adjacent to the gross surface of the specimen.

A. Pyrolytic Graphite

In our studies, we have selected a form of carbon which minimizes the structural uncertainties mentioned in (1) above, yet which can be easily obtained and fabricated into the proper shapes for the experiments. The specimens are pyrolytic graphite, which is a synthetic material possessing many of the properties of naturally occurring single crystal graphite.

The graphitic structure consists of widely spaced layers or planes called basal planes. The carbon atoms in these layers are chemically bound to each other and form a hexagonal mesh in which the carbon-carbon distance is 1.42 Å. Basal planes are arranged in an ABAB... stacking sequence and are separated by 3.35 Å. Interlayer bonding is probably of the van der Waals type. The crystallographic axis perpendicular to the basal planes is the c axis.

If one imagines cutting crystalline graphite parallel to the c axis, two types of planes may be found: "zig-zag" faces consisting of the peaks of the basal plane hexagons and "armchair" faces composed of the sides of the hexagons.[1] Since graphite cannot be cleaved parallel to the c axis, a face consisting of pure "zig-zag" or "armchair" structure cannot be prepared; rather, upon cutting pyrolytic graphite parallel to the c axis, one obtains a mixture of these two faces. This hybrid crystallographic orientation is commonly referred to as the "edge" or "prismatic" face.

Pyrolytic graphite is produced by cracking hydrocarbon gases on a

suitable substrate held at high temperature. The structure grows as cones from nucleation sites on the substrate. Intersection of growth cones forms grain boundaries. To a very high degree, basal planes are oriented parallel to the deposition substrate. The deposit may be grown to substantial thickness, peeled from the substrate, and cut into specimens of any desired shape or orientation.

Essentially all of our experiments were performed with pyrolytic graphite purchased from the Union Carbide Co.[2] This material has a density of ~ 2.17 gms/cm^3, which is ~ 96% of the density of the single crystal. The difference in density between ordinary pyrolytic graphite and single crystal graphite is partially in the interlayer spacing, which is ~ 3.45 Å in the former and 3.35 Å in the latter. In addition, the basal planes of as-fabricated pyrolytic graphite are "kinked", a condition which is manifest as very small pores observable when a prismatic face is viewed under a microscope. Ordinary pyrolytic graphite shows a very highly oriented layered structure when examined by an X-ray diffractometer. However, it is not sufficiently ordered in three dimensions to produce a diffraction pattern when examined by back reflection X-rays.

Annealing pyrolytic graphite at ~ 3000°C for an hour or so shrinks the interlayer spacing towards the theoretical value and straightens out the kinks, yielding a material of 99.5% of theoretical density. We have performed a few experiments with annealed pyrolytic graphite.

Neutron activation analysis of the pyrolytic graphite revealed less than 1 ppm of metallic impurities, sodium being the most abundant.

B. The Modulated Molecular Beam Method

The problems of reaction in the gas phase or upon the apparatus walls and the possibility of diffusional limitations to the rate are entirely eliminated by the modulated molecular beam technique. A

molecular beam of the reactant gas is formed by effusion through an array of small channels into a high vacuum. After collimation, the pencil-like ray of non-colliding molecules strikes the heated target, which consists of a piece of pyrolytic graphite with either the basal or the prismatic plane exposed to the beam. The reaction products are analyzed as they are emitted from the solid by a small mass spectrometer located in the vacuum system. The modulated molecular beam technique is applicable only to reactions in which the products are volatile.

The primary information obtained from such an experiment is the ratio of the rate of emission of a particular reaction product from the surface to the rate of impingement of the reactant gas upon the target. This ratio is called the reaction probability. No measurements of the rate of removal of the solid (e.g., weight loss, surface recession) are made. Because of the low equivalent pressure of the reactant molecular beam, a single specimen is sufficient for a complete investigation.

The principal experimental difficulty of molecular beam studies is that the small reaction product signal is buried in a much larger background signal (noise) due to residual gases in the vacuum system. However, by modulating (i.e., mechanically chopping) the reactant molecular beam and applying phase-sensitive detection methods, the weak reaction product signal may be extracted from a noise level which may be as much as 1000 times larger.

In addition to the usual variables of reactant gas pressure and system temperature available in conventional kinetic studies, the modulated beam technique introduces several new variables and provides an additional piece of output information. The controllable variables

of a molecular beam experiment are:

(1) Target (reactant solid) temperature, T_s.

(2) Reactant gas beam intensity (or equivalent pressure), I_o.

(3) Reactant gas beam temperature, T_B. This parameter may be fixed independently of the temperature of the target.

(4) Modulation frequency, ω.

(5) Angle of reactant beam impingement and product sampling. This variable was not exploited in our experiments.

(6) Crystallographic face upon which reaction occurs.

Because the molecular beam moves in a vacuum without undergoing collisions with walls, other gases in the system, or even with itself, the reactant beam may consist of very reactive species such as free radicals or atoms. Similarly, fragile product species such as free radicals or thermodynamically unstable molecules can be measured as readily as stable molecular products.

Introduction of the modulation frequency as a basic kinetic probe is equivalent to "time tagging" the reactant molecules striking the surface. The output signal bears a particular time relationship to the input reactant gas signal. That is, the process of converting from reactant to product on the surface generally requires a measurable amount of time. In the phase sensitive detection method, this "residence time" is translated into a phase lag of the product signal behind the signal due to the reactant gas. Thus the measured reaction probability mentioned at the beginning of this section is in reality a vector; it possesses an amplitude (relative to the signal due to reactant simply scattered from the target) denoted by ε and a phase (again relative to scattered reactant) denoted by ϕ. The information

obtained in the experiment is in the form of a "reaction product vector", $\varepsilon e^{-i\phi}$ (where $i = \sqrt{-1}$). The amplitude factor ε is an apparent reaction probability, which is always less than the true reaction probability because of demodulation. The true reaction probability is the value of ε in the limit of zero modulation frequency, where the phase lag is also zero.

The confluence of theory and experiment occurs in the quantities ε and ϕ, which are measured as functions of all experimental variables. A model of the surface chemical reactions can be utilized to produce theoretical expressions for ε and ϕ as functions of the same experimental variables. Comparison of model calculations and experimental results may be used to decide whether or not a particular mechanism is acceptable, or to deduce the kinetic parameters of an acceptable model (e.g., activation energies or pre-exponential factors of the rate constants describing the elementary steps of the mechanism).

A schematic of the experimental apparatus and the detection electronics is shown in Fig. 1. The reactant gas molecular beam is generated in the beam source, chopped by a rotating toothed disk, and collimated by a small orifice in the vacuum wall. The beam then passes into another vacuum chamber where it strikes the heated target. Scattered reactant gas and reaction product emitted from the target are again collimated to form a product beam which feeds the quadrupole mass spectrometer. The mass spectrometer is placed in its own vacuum chamber for the following reasons: (1) The background pressure in a separate chamber can be kept considerably lower than in the rest of the system, thus reducing the noise from which the desired signal must be extracted and (2) collimating the secondary molecular beam by a hole in the chamber wall serves to insure that the mass spectrometer

behaves as a "once through", density sensitive type of detector.

As a rule, the reaction product output signal from the mass spectrometer (which is tuned to a particular mass number) has an ac amplitude orders of magnitude below the magnitude of the dc background. When viewed on an oscilloscope, there is usually no visual evidence of a periodic signal. The output of the mass spectrometer and the reference signal from the chopper are both fed into the phase sensitive detector system, which consists of the components shown in the bottom of Fig. 1 (in practice, all of these components are incorporated into a single unit, a Princeton Applied Research Lock-in Amplifier Model HR-8). Signal processing by lock-in amplification is described in refs 3 and 4.

Many experimental systems utilizing molecular beams to probe the interaction of gases with solid surfaces have been constructed.[5,6] The majority of these are designed to measure non-reactive gas-solid interactions, and the primary experimental result is an angular distribution of the scattered primary beam. Our system, on the other hand, is designed exclusively for investigating the heterogeneous reactions between a gas and a solid which produce volatile reaction products ("reactive scattering"). Since reaction probabilities are generally less than 10^{-2}, the primary design aim has been to achieve high sensitivity. To this end, the system: (1) is extremely compact, to minimize $1/r^2$ beam spreading losses between beam source and target and between target and mass spectrometer, and (2) utilizes many stages of differential pumping to provide maximum isolation of the mass spectrometer from the gas load of the beam source (only $\sim 10^{-4}$ of the gas emitted by the source contributes to the usable

molecular beam). This design philosophy has produced a system in which reaction probabilities as low as 10^{-5} can be measured.

The extremely compact design of the beam transport system precludes many desirable auxiliary experimental features available on other systems. No provision is made for angular rotation of either the target or the detector; hence angular distributions of scattered beams cannot be measured. The primary beam incidence and product sampling angles are both fixed at 45° from the surface normal and are coplanar. There is no room for surface monitoring equipment such as LEED or Auger electron spectroscopy. There is no provision for velocity selection of the primary beam or energy analysis of the product beam.

II. DESCRIPTION OF THE APPARATUS*

A. Vacuum System

Fig. 2 illustrates the modular design of the vacuum system, in which flange mounted components are inserted like fingers into a glove. Individual components may be dismounted for adjustment or repair without disturbing neighboring parts. The systems consists of three separately pumped vacuum chambers: (1) the source chamber, (2) the target chamber, and (3) the mass spectrometer chamber.

The source chamber is fabricated in the shape of a cross from 7-inch diameter aluminum pipe and is evacuated by a 500 liter/sec oil diffusion pump with liquid nitrogen baffle and gate valve. A mechanical pump with dry trap is used to rough the entire system or to back the diffusion pump. The source chamber contains the multi-channel molecular beam source, the chopper motor and disk, and a small furnace for heating the beam. No attempt is made to keep this chamber "clean"; viton "O" rings, lubrication oil from the chopper motor and diffusion pump oil contribute a hydrocarbon background to this chamber. The remainder of the vacuum system is all-metal and bakeable.

The graphite specimen is mounted on an electron beam heater and enclosed in the target chamber, which is pumped by a 1200 liter/sec ion pump. The reactant molecular beam enters through a 1 mm diameter collimating orifice piercing the wall separating the source chamber and the target chamber. A quadrupole mass spectrometer head is positioned in the target chamber on the axis of the molecular beam to permit monitoring the primary beam composition when the target is retracted. Surface temperature is measured by sighting an optical or an infrared pyrometer on the target through a sapphire view port.

*Additional details are given in ref 7.

Molecules emitted or scattered from the target enter the mass spectrometer chamber via a 2 mm diameter orifice and pass freely through the ionizer of the mass spectrometer. The un-ionized portion of the product beam then passes through a length of bellows to a 240 liter/sec ion pump to which a titanium sublimation pump has been appended. The mass spectrometer head for reaction product detection is mounted on an adjustable bellows for alignment purposes.

Pressures in the various chambers are measured with ionization gauges. Typical pressures are given in Table 1. Under the conditions listed in the table, the equivalent pressure of the typical beam is $\sim 8 \times 10^{-5}$ torr, which is a factor of ~ 1000 greater than the sum of the background pressure in the target chamber and the equivalent pressure on the target due to effusion from the source chamber background gas. Dimensions of the beam flight paths are shown in Fig. 3. A photograph of the apparatus is shown in Fig. 4.

B. Gas Inlet System

Fig. 5 shows the gas inlet system, whose function is to deliver the gas from which a molecular beam is formed. Gas is drawn from a cylinder (or other source) and metered through a variable leak valve. The low pressure gas (several torr) passes first along two tungsten wire electrodes between which an electrical discharge may be maintained to help purify the gas, then flows through a coiled glass liquid nitrogen cold trap containing glass beads.

Following purification, the gas enters an all-glass (or quartz) coaxial tube arrangement. It first flows down a long thin quartz inner delivery tube up to the tip which contains the multichannel source. In some cases, it is desirable to transport the gas rapidly past the source tip. For this flow mode of operation, the excess gas

is pumped out through the outer annular channel, which is protected downstream by a bead-filled coiled cold trap.

The pressure in the source tube is measured by a Wallace Tiernan gauge (0.1 - 20 torr range) or by a thermocouple gauge. Both gauges were calibrated against a trapped McLeod gauge.

The coaxial source tube is centered on the horizontal axis of the 7-inch aluminum cross which forms the source chamber. It enters this chamber through an "O" ring fitting in a glass window on one arm of the cross. The nose of the source tube is held in an "O" ring-lined sleeve located just back of the furnace shown in Fig. 5. Both mounting points are adjustable for aiming the beam at the target (as one would aim a billiard cue).

C. Molecular Beam Source

The molecular beam is generated by gas flow through an array of 70 capillaries 0.05 mm in diameter which had been electron beam milled through a 0.3 mm thick quartz membrane forming the closure of the source tube. The array of capillaries is packed into a spot approximately 1 mm in diameter, so that the beam is generated from what is effectively a point source. The total flow and the angular distribution obtainable from this source have been measured previously.[8] Using this information, the intensity of the molecular beam at the target may be calculated for any source driving pressure, temperature, and type of gas. The maximum attainable beam intensity at the target is 1.3×10^{17} molecules/cm^2-sec, which corresponds to an equivalent pressure of 4×10^{-4} torr. Beam strength is limited by the speed of the diffusion pump on the source chamber, which must handle essentially all of the effusion load from the beam source.

The small furnace that slips over the source tip consists of a boron nitride liner which is threaded internally to hold a platinum heating wire. The furnace liner is enclosed by tungsten foil heat shields and a stainless steel can. A small hole is provided for the beam to emerge. Beam source temperature is measured by a Pt, Pt-Rh 10% thermocouple place at the tip inside the source tube. A regulated power supply is used to heat the source tip up to 1000°C.

D. Beam Modulation and Reference Signal

The molecular beam is chopped by a rotating slotted disk driven by a synchronous motor which is mounted in a water-cooled brass block in the source chamber (see Fig. 2). A Globe two-phase, 6 pole motor with a 3-inch diameter symmetrically cut 6-blade disk provides a molecular beam chopped at twice the frequency of the power driving the motor. Separating motor drive and modulation frequencies prevents pickup of electromagnetic noise from the motor in the output signal of the mass spectrometer. Details on the powering of the chopper motor are given in ref 9. The modulation frequency range is from 2 to 1500 Hz. Because the beam diameter is small compared to the blade width, a nearly square-modulated beam is obtained.

A reference signal at the chopping frequency must be supplied to the phase sensitive detector to enable this device to extract the desired ac component from the mass spectrometer output signal. In other modulated molecular beam systems, a reference signal is obtained by using a light and photocell placed on opposite sides of the chopper blade. Our compact design precluded this method. Instead, the chopper is illuminated from the outside by a synchronized stroboscope flash. By adjusting the delay of the strobe synchronizing signal, the chopper blade may be "stopped" at a particular reference position. The strobe

synchronizing pulse is fed to the reference channel of the lock-in amplifier, which then has a reference frequency and a phase angle reference point with which the output signal from the mass spectrometer is compared. The strobe technique has the added advantage of eliminating two additional pieces of equipment (light and photocell) from the interior of the vacuum system. A more complete description of the strobe reference technique is given in refs 7 and 9.

E. Target Preparation, Mounting, and Heating

Graphite targets in either of the two crystallographic configurations are prepared from disks 15 mm diameter and 5 mm thick cut from bulk pyrolytic graphite. Subsequent shaping and mounting techniques are shown in Fig. 6. The highly anisotropic thermal conductivity of pyrolytic graphite presented a great obstacle to achieving a high and/or uniform temperature across the face of the target.

Since the thermal conductivity in the c direction is ~ 100 times smaller than along the basal planes, heating a basal plane target from the rear is quite difficult, although temperature uniformity is not a problem. The rear face of the target must be kept considerably hotter than the desired front face temperature in order to transfer by conduction the quantity of heat lost by radiation from the exposed front face. This problem was alleviated by removing material from the rear leaving a thin-walled cup as shown in Fig. 6. Even so, the maximum basal plane temperature attainable was 1800°K.

With the prism plane target (shown on the left in Fig. 6), the problem is not attainment of high temperatures but uniformity of temperature. Heat is conducted easily from the rear to the front face but because of the support pins, radial loss of heat to the tantalum can is not uniform. Wherever a support set screw is located,

a dark (i.e., cool) band forms across the target parallel to the basal planes. By fastening the target at the extreme left and right hand edges in Fig. 6, a reasonably large and uniform hot band was obtained. Temperatures up to 2400°K could be routinely attained.

Prism plane targets are also thinned in the same manner, although somewhat less extensively, as shown for the basal planes. The front face of the samples are prepared for reaction studies by a mechanical polishing sequence ending with 1 micron diamond abrasive and Alumet polishing lubricant. Samples were washed with water and methyl alcohol prior to mounting in the target holder. Both types of targets are mounted in the tantalum holder in the same manner: two fixed set screws on one side and a long tungsten spring-loaded pointer to engage a shallow hole on the opposite side hold the target through thermal cycling.

Once installed, the sample is degassed while the system is pumped down and baked at 500°K for 8 hours. The sample is then heated to around 1300°K and subjected to an oxygen beam of about 3×10^{16} molecules/cm^2-sec in order to burn off any disturbed surface material and to obtain a reproducible surface condition. This pre-conditioning occupies about 30 hours and is estimated to remove 2×10^{19} carbon atoms/cm^2 of geometrical surface or 1.5 microns.

The tantalum can visible in Fig. 2 supports the target by the set screws just described and also houses the electron beam heater. The entire assembly is mounted on a linear motion feed-through attached to a 6-inch flange on the wall of the target chamber. The coaxial electron beam heater is fabricated of tantalum with alumina insulators. A flat spiral or "pancake wound" tungsten filament is heated resistively and biased to a high potential by a 10 kw power supply.

Target temperature is measured by Micro Optical disappearing filament pyrometer. The emissivity at 0.65μ of pyrolytic graphite was taken to be 0.76 for both crystallographic orientations.[2, 10] The target face is viewed at normal incidence through a sapphire window which has an 87% transmissivity for the 0.65 micron wavelength of the optical pyrometer. Fogging of the window by vaporized graphite is minimized

by an electromagnetically operated shutter placed in the vacuum chamber just behind the window.

The maximum attainable temperatures cited above are limited by carbon vaporization from the rear face of the target, which ultimately consumes the target more rapidly than the chemical reaction occurring on the front face.

F. The Detection System

An early model Electronics Associates Inc. quadrupole mass spectrometer head and ionizer is used for beam monitoring (see Fig. 2). A Granville-Philips spectrometer head is utilized in the mass spectrometer chamber. Both probes are powered (alternately) by a single EAI Quad 250 electronics package. To minimize center-of-mass location errors in re-tuning the spectrometers for different species, a power supply was connected to the spectrometer center mass circuit and provided with switch-selected 10-turn programming resistors that could be set and locked to a desired mass number.

The mass spectrometers are operated in the low mass range (0 - 100 AMU) with the resolution at mass 28 adjusted so that the valley between adjacent peaks just touches the base line. Voltage on the 14 stage electron multiplier is adjusted from 2.5 to 3.0 kV to provide the best signal-to-noise ratio.

The modulated signal current from the spectrometer is dropped across a 1 megohm resistance and presents a voltage which is then processed in analog form by the lock-in amplifier. Due to stray and cable capacitances, the voltage response lags the current excitation and a phase shift and amplitude attenuation of the electrical signal occurs. A circuit model permitting corrections for this effect was

formulated[9]; at 1000 Hz, for example, the complex impedance produces a 25° phase shift and a 10% amplitude attenuation. Data taken at different frequencies were corrected for the perturbation introduced by the complex impedance of the external circuit.

There are three means of processing the signal from the mass spectrometer: (1) Complete wave shape determination by devices such as a waveform eductor or a computer of average transients (CAT); (2) Digital (pulse) counting techniques; and (3) Determination of the phase and amplitude of the first Fourier component of the signal waveform by lock-in detection.

Method (1) was used infrequently; it suffers from the difficulty of correcting the complete waveform for complex impedance effects, and the substantial analytical problem of comparing reaction models to a waveform instead of some quantitative measure of the wave (such as its Fourier components).

Method (2) was rejected because the very large pulse count rates at the mass numbers of interest in our experiments produced considerable counter dead time. In addition, our mass spectrometer head had not been especially shielded to isolate the signal from the rf power to the rods. These problems could have been solved, but the effort was not deemed worthwhile for the present experiments.

Consequently, phase sensitive processing by means of a lock-in amplifier was chosen. The phase and amplitude information provided by the lock-in amplifier are those of the first Fourier component of the complete signal waveform. These quantities are directly provided by the theory for a particular surface mechanism.

The input signal is brought into the type A preamplifier of the

lock-in amplifier. The reference channel is operated in the "automatic" mode driven by negative pulses synchronized to the stroboscope drive. Main tuning is accomplished with a dual beam oscilloscope by matching the negative trigger pulse and the zero crossing of the calibrator signal derived from the reference channel.

In the lock-in amplifier the mass spectrometer signal is passed through a narrow band amplifier tuned to the modulation frequency, thereby selecting only the first Fourier component for subsequent processing. The signal is then sent to a synchronous demodulator where it is compared with the reference signal which is provided with an adjustable phase control. The dc output reading of the lock-in amplifier, s, varies with phase setting of the reference signal, ϕ_{ref}, according to:

$$s = S \cos (\Phi - \phi_{ref}) \qquad (1)$$

There are various ways of operating the lock-in amplifier to extract the amplitude S and the phase angle Φ of the first Fourier coefficient of the mass spectrometer signal. In the conventional mode of operation, the lock-in amplifier is frequency-tuned to the signal of interest then the phase control is adjusted to maximize the signal. According to Eq. (1), the lock-in output is equal to the amplitude of the input signal and the phase setting corresponds to the phase angle of the signal. However, this method is relatively insensitive to phase setting, because tuning is performed around the maximum at the relatively flat peak of a cosine curve. A more sensitive method of operation is to adjust the phase for null signal (i.e., 90° out of phase), which involves operation about the zero

crossing of the cosine curve.

A better approach developed for the present experiments is to use two lock-in amplifiers connected in parallel at the electron multiplier. The two lock-ins simultaneously display the signal magnitudes at phase settings separated by 90°. One unit is set to give the component of the input signal in phase with the reference signal (i.e., $\phi_{ref} = 0$). This reading is denoted by s_0. The other unit is set to give the signal at a phase 90° from the reference signal ($\phi_{ref} = 90°$). The output from this unit is denoted by s_{90}. Since the output of a lock-in amplifier varies with phase setting according to Eq. (1), the amplitude and phase angle of the signal fed to the pair of amplifiers is:

$$S = \sqrt{s_0^2 + s_{90}^2} \tag{2a}$$

$$\Phi = \tan^{-1} (s_{90}/s_0) \tag{2b}$$

The output signals s_0 and s_{90} are smoothed by integrating in a 12 db/octave filter in the lock-in amplifier using a time constant of 1 to 100 sec. Very steady signals are read on the panel meter of the amplifier or on a digital voltmeter. Weaker signals are recorded on a strip chart recorder.

III. DATA INTERPRETATION

A. Obtaining the Apparent Reaction Probability and the Reaction Phase Lag

The measured quantities S and Φ cannot be compared directly with the predictions of theoretical models of the surface process because: (1) S and Φ contain instrumental factors peculiar to the experiment, and (2) they are influenced by other phenomena not germane to the surface interaction. Most of the extraneous influences on S and Φ are removed by comparing the amplitude and phase angle of a reaction product signal to the same quantities measured for the reactant beam which has simply been scattered from the target. The parasitic phenomena which remain after this comparison are handled by analytic correction procedures.

Consider the measured phase angle Φ. It consists of the following components:

(1) A mechanical phase shift, ϕ_{mech}, occurs because the chopper blade does not cross the reference "position" at the same time that the chopper crosses the axis of the molecular beam.

(2) Transformation of the mass spectrometer output current to a voltage signal adds a complex impedance phase lag ϕ_Z, which is a function of frequency alone. This effect is removed analytically.

(3) Phase lags occur due to finite molecular transit times between the chopper and the target and between the target and the mass spectrometer. These lags are denoted by ϕ_{tr}.

(4) A phase lag due to the residence time on the surface, designated by ϕ.

The measured phase angle must be stripped of the first three components; information on the surface processes is contained only in component (4).

Of the three parasitic phase lags, only (3), the transit effect, needs further consideration. As an example of the importance of this phenomenon, consider a molecule traversing a 4 cm flight path (typical of our apparatus) and requiring ~ 10^{-4} secs to do so. At a modulation frequency of 1000 Hz, this delay represents a phase lag of ~ 35°. Since phase angles of strong signals can be measured to ±1°, transit corrections are mandatory. Even with short beam transport paths, transit delay ultimately sets an upper limit to the usable modulation frequency, and hence a lower limit to the surface residence times which can be detected by the apparatus.

The phase shift and the amplitude attenuation caused by molecular transit have been computed for square-modulated Maxwellian beams by Harrison et al.[11] Similar theory has been exploited to determine the velocity distribution in beams from channel sources.[9] In the present experiment, we wish to eliminate transit effects from the data by analytical means. To do so, the molecular speed spectrum in both the primary and product molecular beams is assumed to be Maxwellian (the small deviation from Maxwellian behavior noted in channel beams[9] is neglected). The transit effects are functions of the modulation frequency, the flight path d, the beam temperature and the molecular weight M. These quantities appear as the parameter:

$$X = \frac{\omega d}{v_{MP}} \tag{3}$$

where v_{MP} is the most probable speed of the Maxwell-Boltzmann distribution:

$$v_{MP} = (2RT/M)^{1/2} \quad (4)$$

R is the gas constant (Boltzmann's constant times Avogadro's number). Harrison et al[11] have prepared tables from which the transit phase lag, $\phi_{tr}(X) = \phi_{tr}(d, \omega, M, T)$ and the transit amplitude attenuation $A_{tr}(X) = A_{tr}(d, \omega, M, T)$ can be obtained.*

The signal due to reaction product is compared to the signal obtained from the room temperature (300°K) reactant gas which has been simply scattered from a room temperature target. The measured phase angle of the scattered reactant beam may be written as

$$\Phi_R = \phi_{mech} + \phi_Z(\omega_o) + \phi_{tr}(d_1, \omega_o, M_R, 300) + \phi_{tr}(d_2, \omega_o, M_R, 300) \quad (5)$$

where the subscript R denotes scattered reactant, ω_o is the modulation frequency at which this signal was measured, and M_R is the molecular weight of the reactant species. d_1 and d_2 are the chopper-to-target and target-to-detector distances, respectively. They are shown in Fig. 3.

Similarly, the measured phase angle of the product signal can be broken down into components:

$$\Phi_P = \phi_{mech} + \phi_Z(\omega) + \phi_{tr}(d_1, \omega, M_R, T_B) + \phi_{tr}(d_2, \omega, M_P, T_s) + \phi \quad (6)$$

where P denotes the product species and ω is the modulation frequency at which the reaction product signal was measured. The transit

*Actually, the transit correction from chopper-to-target pertains to the flux, while that from target-to-detector pertains to the number density. To avoid complication of the notation, this distinction is not made in the text, although it was observed in applying the transit corrections to the data.

correction allows for heated reactant ($T_B > 300°K$), but assumes that the product species is emitted from the target at the temperature of the solid. Note that the first transit term in Eq. (6) applies to the reactant species (which actually travels from the chopper to the target) while the second term applies to the product species which has been created by the surface reaction.

The reaction phase lag is obtained by subtracting Eq. (5) from Eq. (6):

$$\phi = (\Phi_P - \Phi_R) - \left[\phi_Z(\omega) - \phi_Z(\omega_o)\right] - \left[\phi_{tr}(d_1, \omega, M_R, T_B) - \phi_{tr}(d_1, \omega_o, M_R, 300)\right] - \left[\phi_{tr}(d_2, \omega, M_P, T_s) - \phi_{tr}(d_2, \omega_o, M_R, 300)\right] \quad (7)$$

The phase angle difference $(\Phi_P - \Phi_R)$ is obtained by applying Eq. (2b) to the outputs of the lock-in amplifiers for the measurements on the scattered reactant and product beams. The second bracketed term in Eq. (7) is obtained analytically.[9] Except for a frequency scan (when $\omega \neq \omega_o$) or for hot beam experiments ($T_B > 300°K$), the chopper-to-target transit correction vanishes. The last bracketed term in Eq. (7) represents the target-to-detector correction. It never vanishes because the emitted product species is invariably hotter than the impinging reactant and the reactant molecular weight differs from the product molecular weight. With graphite reactions, however, these two molecular weights are not greatly different, and the transit correction is substantial only at very high chopping frequencies.

Similar corrections are applied to the measured signal amplitudes. As in the case of the phase lag, the product signal amplitude is compared to the amplitude of the signal obtained when a room temperature

reactant beam is scattered from a room temperature target. We also make one additional correction at this point; theoretical models of the surface process predict fluxes of various products from the target surface, whereas the mass spectrometer detector measures the number density of the species in the ionizer. The molecular current in the flow-through ionizer, which is proportional to the flux of the species emitted from the target surface, is given by the product of the number density and the mean molecular speed. Since the mean molecular speed is proportional to the square root of the temperature, the measured signal amplitude, S, may be converted to represent a flux rather than a number density by multiplying by $T^{1/2}$. The signal amplitudes are also corrected for transit attenuation and for attenuation due to the impedance of the external circuitry. The ratio of the product and reactant signals so corrected is the measured apparent reaction probability:

$$\varepsilon = \frac{S_P}{S_R}\left(\frac{T_s}{300}\right)^{1/2} \frac{A_Z(\omega_o)}{A_Z(\omega)} \frac{A_{tr}(d_1, \omega_o, M_R, 300)}{A_{tr}(d_1, \omega, M_R, T_B)} \frac{A_{tr}(d_2, \omega_o, M_R, 300)}{A_{tr}(d_2, \omega, M_P, T_s)} \tag{8}$$

where S_R and S_P are the measured signal amplitudes for the scattered reactant and the product as determined from the lock-in amplifier readings and Eq. (2a). $A_Z(\omega)$ is the calculated attenuation due to complex impedance.

The quantities ϕ and ε of Eqs. (7) and (8) describe the direction and magnitude of the "reaction product vector". They represent the sole pieces of information which the modulated beam experiment provides. They have been purged of all extraneous effects and represent only the

response of the surface proper to the modulated reactant beam. They may be directly compared to theoretical models of the surface processes.

B. The Link Between Measurements and Theory

Periodic interruption of a reactant molecular beam impinging on a target introduces a periodic variation in the surface concentration of intermediates participating in the overall surface reaction. One of the surface species vaporizes to provide the product molecular beam which is analyzed by the mass spectrometer, and ultimately yields the experimental quantities ε and ϕ discussed in the preceding section. The flux of product molecules emitted from the surface depends upon the surface concentration of the species. The theoretical description of the surface processes must predict the time variation of the concentration of the desorbing species. In this section, we show how the periodic surface concentration is related to ε and ϕ. Particular reaction models are required to describe the surface concentration; a few of these are considered in the following section.

A general scheme has previously been developed to enable ε and ϕ to be predicted for any class of surface reaction.[12] In this method, the complete solutions to the non-steady state equations representing surface mass balances for each identifiable reaction intermediate are obtained. The resulting solutions are then expanded in a Fourier series and the phase and amplitude of the fundamental mode identified with the quantities ε and ϕ. For non-linear surface processes, this "brute force" method is, as far as we know, the only means of treating the problem. For linear processes, however, a considerably simpler method may be employed.

Lock-in detection extracts only the fundamental Fourier component of a signal. In a linear system, each Fourier component behaves independently of the others; therefore, only the response of a postulated surface mechanism to the fundamental component of the modulated molecular beam needs to be evaluated.

Instead of considering a square, trapezoidal or other complex primary beam gating function, we consider only the response of the surface to a simple sinusoid, or, in complex notation, to the gating function:

$$g(t) = \bar{g}e^{i\omega t} \tag{9}$$

where $\bar{g}$ is the coefficient of the first Fourier term of the actual gating function.

Consider the response due to the simple scattering of the primary reactant beam from the target (both at 300°K). The rate at which reactant molecules impinge upon a unit area of the target is $I_o g(t)$, where I_o is the intensity of the molecular beam striking the target. All of these are instantaneously reflected. The time dependent mass spectrometer response to the scattered beam may be written as:

$$i_R(t) = \frac{\beta_R I_o g(t)}{\sqrt{300}} \tag{10}$$

where $i_R(t)$ is the electric current signal sent by the mass spectrometer to the lock-in amplifier. The $\sqrt{300}$ term in the denominator reflects the density-sensitive nature of the detector. The parameter β_R is an instrumental constant which includes the following:

(1) the target-to-detector collimation geometry

(2) the angular distribution of the scattered beam

(3) the ionization and transmission coefficients of the mass spectrometer and the first dynode efficiency and gain of the electron multiplier.

The current described by Eq. (10) is fed to the lock-in amplifier, which, however, responds only to the fundamental mode of $i_R(t)$. Since the reaction phase lag of the scattered reactant beam is (by definition) equal to zero, the lock-in amplifier produces the signal amplitude S_R at zero phase lag:

$$S_R = \frac{\beta_R I_o \bar{g}}{\sqrt{300}} \tag{11}$$

Consider now the signal due to the reaction product. This species desorbs from the surface at a rate given by $k_d n(t)$, where k_d is the desorption rate constant, and $n(t)$ is the instantaneous surface concentration of the product species. The mass spectrometer signal resulting from the desorption flux is:

$$i_p(t) = \frac{\beta_p k_d n(t)}{\sqrt{T_s}} \tag{12}$$

The lock-in amplifier responds to this current excitation with an output of amplitude S_p lagging the scattered reactant signal by ϕ:

$$S_p e^{-i\phi} = \frac{\beta_p k_d \bar{n}}{\sqrt{T_s}} \tag{13}$$

where the complex quantity $\bar{n}$ is the first Fourier coefficient of $n(t)$. Clearing the temperature terms from the denominators, division of Eq. (13) by Eq. (11) gives the reaction product vector:

$$\varepsilon e^{-i\phi} = \frac{S_p}{S_R}\left(\frac{T_s}{300}\right)^{1/2} e^{-i\phi} = \left(\frac{k_d \bar{n}}{I_o \bar{g}}\right) \tag{14}$$

In obtaining Eq. (14) from Eqs. (11) and (13), the ratio of instrumental constants, β_p/β_R, has been taken as unity for the following reasons: Aside from the species-dependent mass spectrometer efficiencies included in β (which are not significantly different

for reactant and product), the possibility of substantial differences between the angular dependence of the scattered reactant and the desorbed product fluxes represents the main source of difference between β_P and β_R. To eliminate this effect, the reactant must be scattered from the surface with the same cosine distribution which (presumably) characterizes product desorption. To insure diffuse reflection, the scattered reactant signal is measured for a room temperature beam and a room temperature target. At low temperatures, even highly polished targets should have adsorbed enough impurities from the background gases to give diffuse reflection of impinging molecules.

Eq. (14) provides the link between theory and experiment for a linear reaction mechanism. Solution of the surface mass balances for the fundamental component of the surface concentration of the desorbing product yields theoretical values of ϵ and ϕ by substitution into Eq. (14). These may then be compared with the experimental values obtained from Eqs. (7) and (8).

C. Application to Simple Surface Mechanisms

We consider in this section three surface processes which illustrate the manner in which ϵ and ϕ are determined. These cases have been considered previously by the more cumbersome "brute force" method.[12] However, the present illustrations serve to demonstrate the ease with which linear surface mechanisms can be handled to yield the reaction product vector. Also, some of the features of the theoretical models may serve as guidelines in the often tedious reverse process; that is, trying to fit a model to experimentally determined apparent reaction probabilities and reaction phase lags.

1. Simple Adsorption-Desorption

A beam of diatomic molecules A_2 impinges upon a surface. A fraction η sticks to form an adsorbed species A(ads) which desorbs with a rate constant k_d to form gaseous A (surface recombination is neglected). This mechanism is depicted by:

$$A_2(g) \longrightarrow 2A(ads) \longrightarrow 2A(g) \tag{15}$$

The surface mass balance describing the time variation of the surface concentration of A(ads) (which is denoted by n) is:

$$\frac{dn}{dt} = 2\eta I_o g(t) - k_d n \tag{16}$$

Since the process is first order and only the fundamental mode of the surface concentration is desired, g(t) may be described by Eq. (9) and the concentration of adsorbed A by:

$$n(t) = \bar{n} e^{i\,\omega t} \tag{17}$$

Substituting Eq. (9) and (17) into Eq. (16) and solving yields:

$$\bar{n} = \frac{2\eta I_o \bar{g}}{k_d + i\omega} \tag{18}$$

Converting the complex quantity on the right hand side of Eq. (18) to polar form and substituting into Eq. (14) shows that:

$$\varepsilon = \frac{2\eta}{\left[1+\left(\omega/k_d\right)^2\right]^{1/2}} \tag{19}$$

and

$$\phi = \tan^{-1}(\omega/k_d) \tag{20}$$

Eq. (19) illustrates what is meant by "amplitude demodulation".

The true reaction probability for the simple adsorption-desorption process is 2η. The apparent reaction probability is reduced from this value by the factor $[1+(\omega/k_d)^2]^{1/2}$. At very large frequencies, the apparent reaction probability approaches zero. This does not mean that the dissociation process is not occurring - rather, it means that the surface process is slow compared to the chopping speed. The modulated detection method no longer has an ac component of the desorbed product signal to work with.

Eqs. (19) and (20) also illustrate the general rule that signals characterized by large reaction phase lags are less likely to be observed than signals with phase lags near zero. Eq. (20) shows that if ϕ, is to be large, than ω/k_d must also be large. However, large ω/k_d demodulates the apparent reaction probability. If ε is very small for whatever reason, the signal is difficult to detect at all, irrespective of its phase.

Eq. (20) suggests that a plot of tan ϕ against ω should produce a straight line of slope $1/k_d$. Similarly, Eq. (20) predicts a linear variation of ε^{-2} with ω^2 exhibiting a slope $(2\eta k_d)^{-1}$. A phase-amplitude measurement at a single temperature permits the sticking probability and the desorption rate constant to be determined. The desorption rate constant depends upon temperature according to:

$$k_d = A_d e^{-E_d/RT_s} \qquad (21)$$

where A_d is a frequency factor and E_d is the activation energy for desorption. An Arrhenius plot of the apparent reaction probability against surface temperature should have as its slope:

$$\frac{\partial \ell n \varepsilon}{\partial (1/T_s)} = - \frac{E_d}{R} \frac{(\omega/k_d)^2}{1+(\omega/k_d)^2} \tag{22}$$

At high frequencies (or low temperatures), $(\omega/k_d) >> 1$ and the slope of the Arrhenius plot gives E_d directly. Once E_d is known the pre-exponential factor may be determined from the known value of k_d at any temperature.

2. The Series Process

Consider the process in which A_2 chemically combines with atoms of the solid S to form reaction product SA according to the scheme:

$$A_2(g) + 2S \longrightarrow 2SA(ads) \xrightarrow{k_1} 2SA^+ \xrightarrow{k_d} 2SA(g) \tag{23}$$

In this mechanism, adsorbed SA transforms to a desorption precursor state SA^+ by a step described by a first order rate constant k_1. Desorption of SA^+ proceeds with a rate constant k_d. Surface mass balances for the intermediates SA(ads) and SA^+ (denoted by n' and n respectively) may be written as:

$$\frac{dn'}{dt} = 2\eta\, I_o g(t) - k_1 n' \tag{24}$$

$$\frac{dn}{dt} = k_1 n' - k_d n \tag{25}$$

Substituting trial solutions $\bar{n}' e^{i\,\omega t}$ for n'(t) and $\bar{n} e^{i\,\omega t}$ for n(t), the response of the surface to the gating function of Eq. (9) may be expressed in terms of the reaction product vector:

$$\varepsilon = \frac{2\eta}{\left[1+(\omega/k_d)^2\right]^{1/2} \left[1+(\omega/k_1)^2\right]^{1/2}} \tag{26}$$

$$\phi = \tan^{-1}(\omega/k_d) + \tan^{-1}(\omega/k_1) \tag{27}$$

If either one of the steps in (23) is very fast, the remaining step becomes rate determining and the behavior of ε and ϕ reduces to that of simple adsorption-desorption.

By eliminating the modulation frequency between Eqs. (19) and (20) and between (26) and (27), the reaction product vectors for the two processes may be represented on polar plots. As shown in Fig. 7, the locus of reaction vector describes a curve on the diagram. The shape of each curve is characteristic of the surface processes involved. In the simple adsorption-desorption case depicted in Fig. 7a, the reaction vector traces a semicircle from the true reaction probability at zero phase lag at low frequency to complete demodulation ($\varepsilon = 0$) and a 90° phase lag at very high frequencies.

Fig. 7b shows a polar plot of the reaction vector for the special case of the series process in which $k_1 = k_d$. The characteristic feature which signifies a series process is that the phase lag can exceed 90°; complete demodulation occurs as the phase approaches 180°.

3. Diffusion-Limited Surface Processes

Recent molecular beam surface reaction studies suggest that heterogeneous reactions may be influenced by diffusional processes either on the surface[13] or in the bulk of the solid. Consider the situation in which a dissociatively adsorbed gas may dissolve and diffuse into (and out of) the semi-infinite bulk solid in addition to desorbing as atoms from the surface. This mechanism may be written as:

$$\begin{array}{ccccc} A_2(g) & \longrightarrow & 2A(ads) & \longrightarrow & 2A(g) \\ & & \downarrow\uparrow & & \\ & & 2A(sol'n) & & \end{array} \qquad (28)$$

Denoting the surface concentration of A by n(t) and the concentration in the bulk solid by C(x, t) (x = distance into the solid normal to the surface) and assuming that the bulk concentration of A just beneath the surface to be related to the concentration of adsorbed A by a solubility coefficient H, we may write:

$$C(0, t) = Hn(t) \tag{29}$$

The surface balance on A(ads) reflects the loss term due to solution into the bulk solid:

$$\frac{dn}{dt} = 2\eta I_o g(t) - k_d n(t) + D\left(\frac{\partial C}{\partial x}\right)_0 \tag{30}$$

where D is the diffusion coefficient of A in the solid. When n(t) is expressed in terms of C by Eq. (29), Eq. (30) serves as a boundary condition to the bulk diffusion equation, which is:

$$\frac{\partial C}{\partial t} = D\frac{\partial^2 C}{\partial x^2} \tag{31}$$

As in the previous cases considered, the driving function is given by Eq. (9) and the response is assumed to be of the form $\bar{C}(x)e^{i(\omega t-\phi(x))}$. Eq. (31) is then solved subject to Eq. (30) as one boundary condition and a condition requiring finite concentration at large x as the other. Proceeding as in the previous examples, the apparent reaction probability and the reaction phase lag are found to be:

$$\varepsilon = \frac{2\eta}{\left\{\left(1+s\sqrt{\frac{\omega}{k_d}}\right)^2 + \left(\frac{\omega}{k_d} + s\sqrt{\frac{\omega}{k_d}}\right)^2\right\}^{1/2}} \tag{32}$$

$$\phi = \tan^{-1}\left[\frac{\left(\frac{\omega}{k_d}\right) + S\sqrt{\frac{\omega}{k_d}}}{1 + S\sqrt{\frac{\omega}{k_d}}}\right] \tag{33}$$

where:

$$S = \left(\frac{H^2 D}{2k_d}\right)^{1/2} \tag{34}$$

As the solution-diffusion parameter S approaches zero, the apparent reaction probability and reaction phase lag reduce to the expressions for simple adsorption-desorption.

For strong solution-diffusion control ($S \to \infty$), a constant 45° phase lag is obtained and the apparent reaction probability varies as the inverse square root of the modulation frequency. Similar behavior is calculated for the temperature response of the earth's surface due to the diurnal heating by the sun.[14] Under conditions where the distinctive 45° phase shift is observed the amplitude is very highly demodulated. In effect, diffusion into and out of the bulk acts like a flywheel in the process, which, by its sluggish time response, prevents the surface from reacting quickly to the periodic supply of reactant gas.

4. A General Phase-Amplitude Relation for Linear Processes

An interesting relation between reaction phase lag and apparent reaction probability can be obtained by analogy to linear network analysis. The effect of passing a sinusoidal signal through a linear electrical network is multiplication of the signal by e^{A+iB}. In the modulated molecular beam case considered here, the analog of the electrical circuit is the surface and A corresponds to $\ln\varepsilon$ and B to ϕ. The relation between A and B from electric circuit theory[15] may be written as the following relation between ε and ϕ:

$$\phi(\omega) = \frac{1}{\pi}\int_{-\infty}^{\infty} \frac{d\ell n\varepsilon}{du}\, \ell n\left[\coth\frac{|u|}{2}\right]du \qquad (35)$$

where $u = \ln(\omega'/\omega)$ and u or ω' are dummy variables of integration. Eq. (35) states that <u>if</u> the apparent reaction probability is known for all frequencies from 0 to ∞, the reaction phase lag may be calculated. For example, if $\varepsilon \sim \omega^{-1/2}$, as in the diffusion-limited surface process with $h \to \infty$ discussed in the preceeding section, Eq. (35) shows that $\phi = 45°$.

Eq. (35) is not particularly useful in the determination of ε and ϕ for a particular reaction model, since these two quantities are obtained simultaneously from the theory. However, the formula may have some utility as a consistency check on experimental data. If the surface processes are linear, ε and ϕ must satisfy Eq. (35). In this role, Eq. (35) is analagous to the Gibbs-Duhem relation in solution thermodynamics.

TABLE 1 Vacuum Performance of the System

Chamber	Base pressure, torr	Pressure under normal beam load, torr[a]
Source tube	10^{-4}	4
Source chamber	2×10^{-7}	8×10^{-5}
Target chamber	2×10^{-9}	4×10^{-8}[b]
Mass spectrometer chamber	8×10^{-10}	2×10^{-9}

[a]for beam intensity striking target of ~ 3×10^{16} molecules/cm^2-sec.

[b]with target at ~ 2000°C, pressure rises to 8×10^{-8} torr.

LITERATURE CITED

1. J. M. Thomas and E. E. G. Hughes, Carbon 1, 209 (1964).
2. Data Sheet, PG (Pyrolytic Graphite) High Temperature Materials, Inc., Lowell, Mass. 01852.
3. O. C. Chaykowsky and R. D. Moore, Research/Development, p 32 April, 1968.
4. C. A. Nittrouer, Electronic Instrument Digest, October, 1968.
5. R. P. Merrill, Catalysis Reviews 4, 115 (1970).
6. G. A. Somorjai, Principles of Surface Chemistry, Prentice-Hall (1971).
7. R. H. Jones, Ph D. Thesis, AEC Report LBL-104 (1971).
8. R. H. Jones, D. R. Olander, and V. R. Kruger, J. Appl. Phys. 40, 4641 (1969).
9. W. J. Siekhaus, R. H. Jones, and D. R. Olander, J. Appl. Phys. 41, 4392 (1970).
10. F. M. Wachi, and D. E. Gilmartin, Carbon 8, 141 (1970).
11. H. Harrison, D. G. Hummer, and W. L. Fite, J. Chem. Phys. 41, 2567 (1964).
12. D. R. Olander, Proc. of the Fourth Intern. Materials Symp., (Wiley, 1969) pp. 45-1 to 45-50, G. A. Somorjai, ed.
13. R. A. Krakowski, and D. R. Olander, J. Chem. Phys. 49, 5027 (1968).
14. H. S. Carslaw and J. C. Jaeger, Conduction of Heat in Solids, 2nd Ed., p 65, Oxford (1959).
15. H. W. Bode, Network Analysis and Feedback Amplifier Design, (D. Van Nostrand, New York 1945) Ch. 14, p. 313.

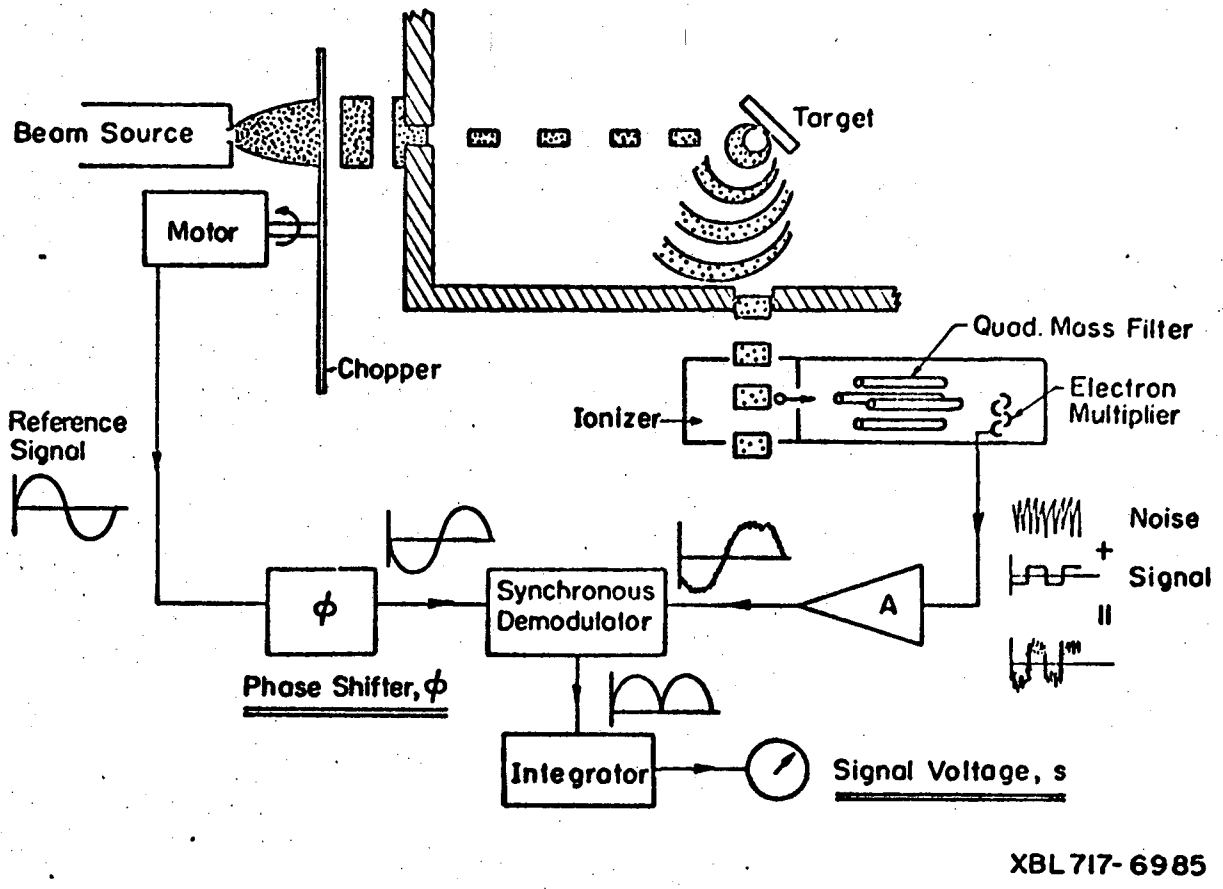

Fig. 1. Schematic of a modulated molecular beam system for the study of gas-solid reactions.

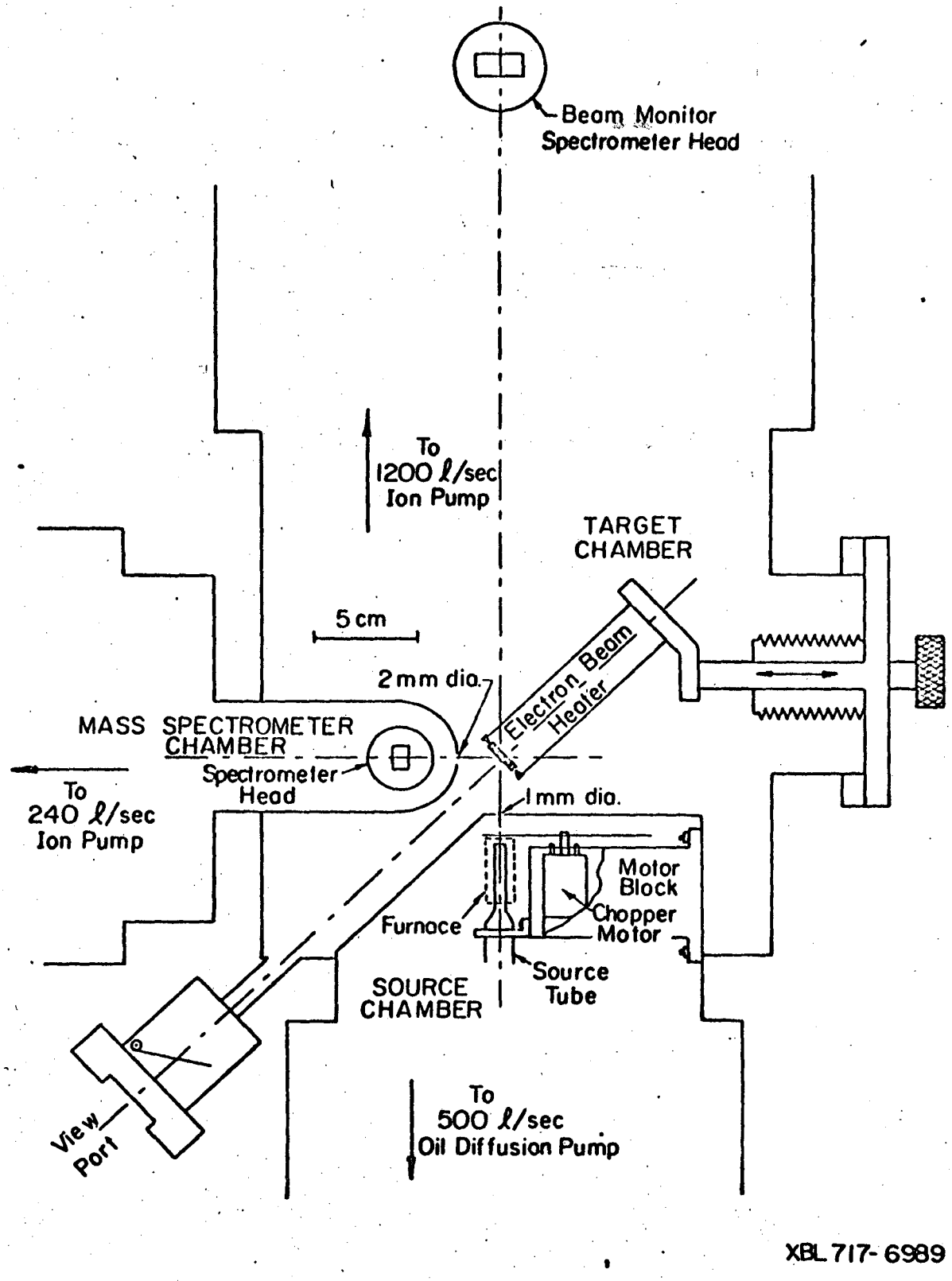

Fig. 2. Schematic of apparatus.

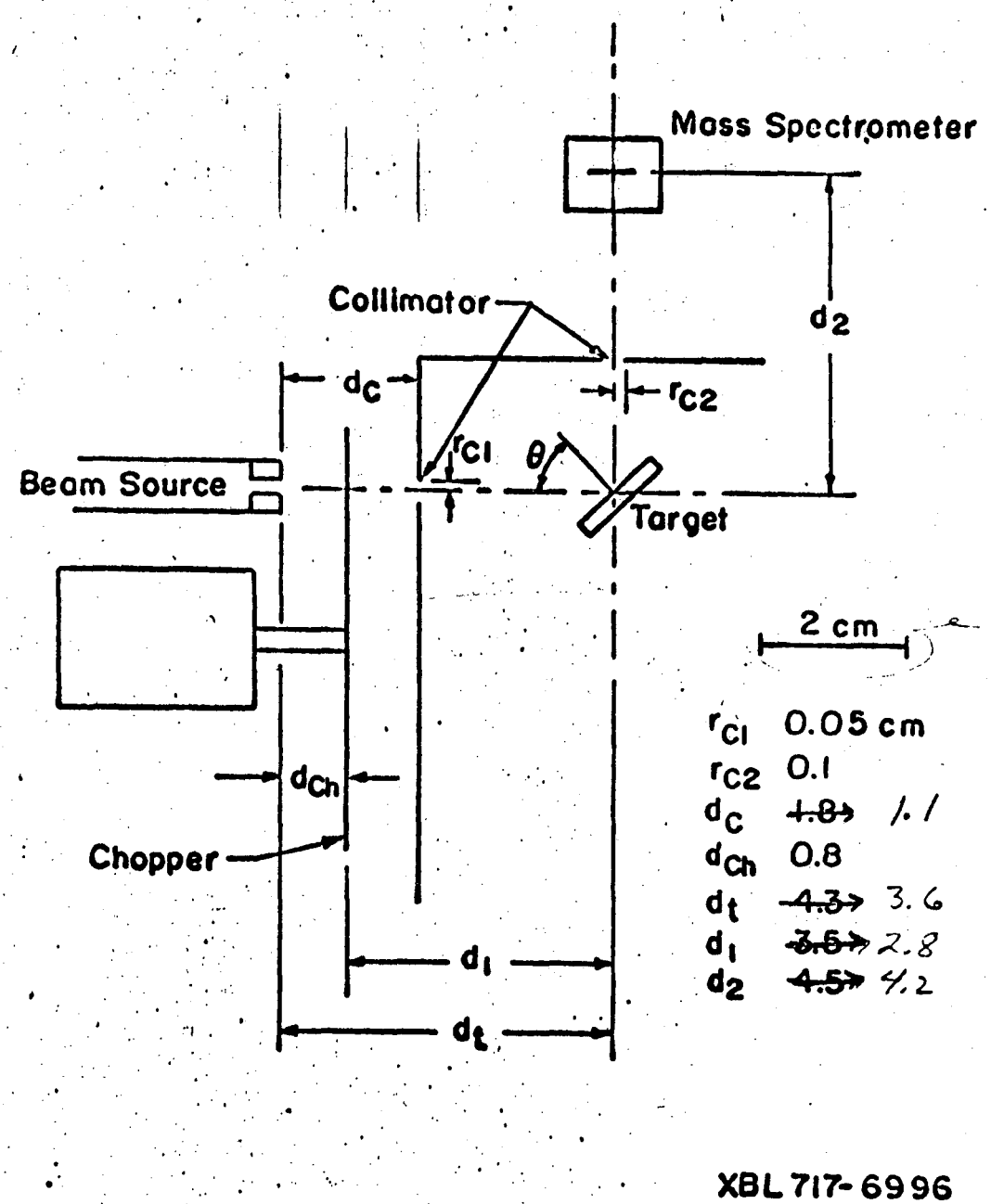

Fig. 3. Geometry of beam transport paths.

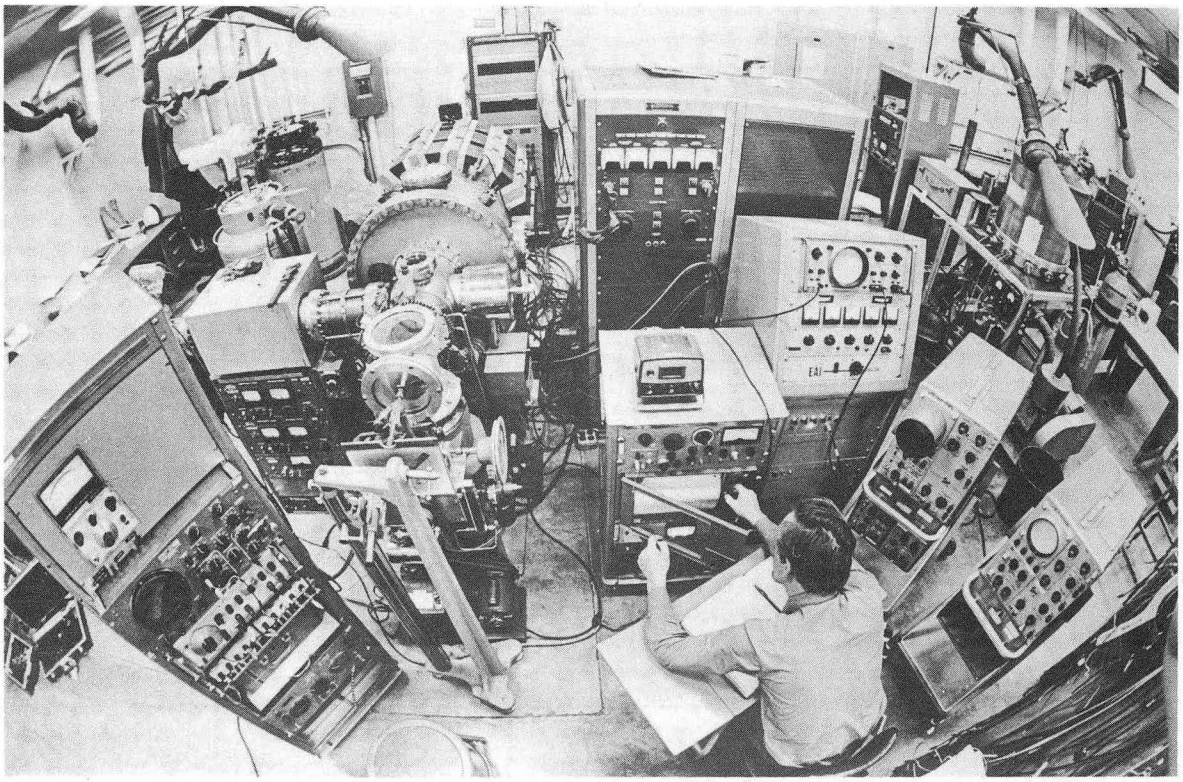

XBB 715-2247

Fig. 4. Photograph of the system.

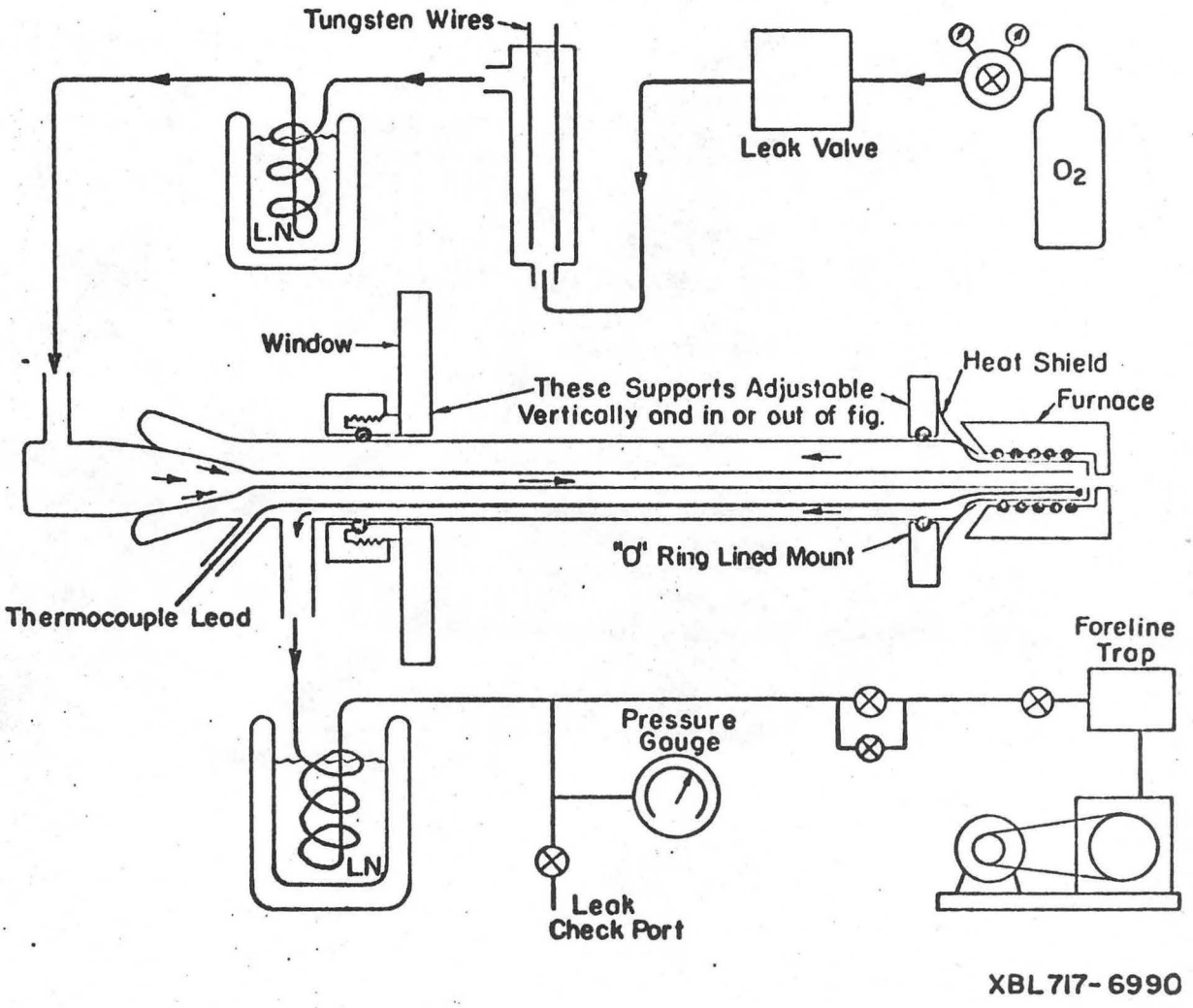

Fig. 5. The gas inlet system.

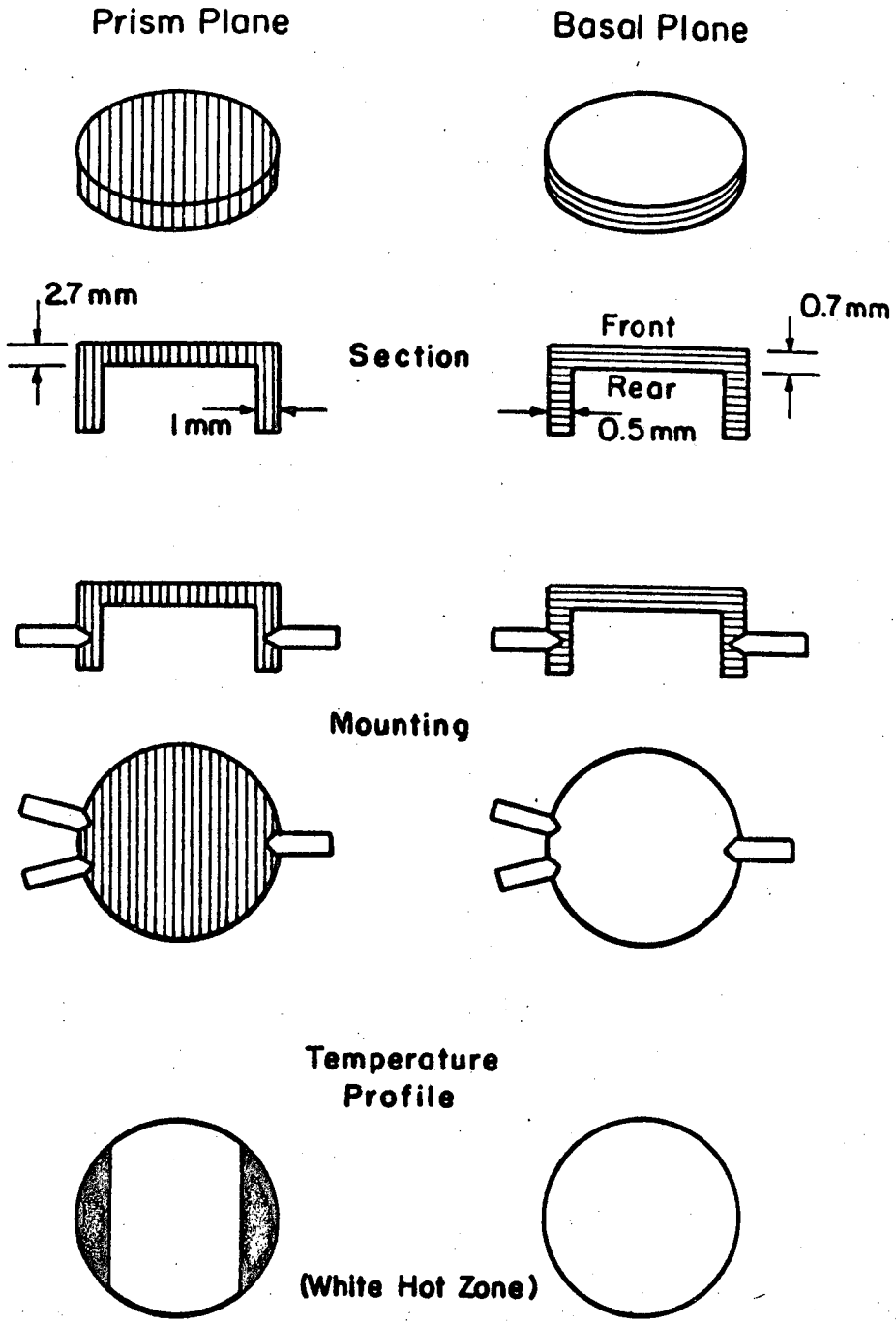

Fig. 6. Preparation of pyrolytic graphite targets.

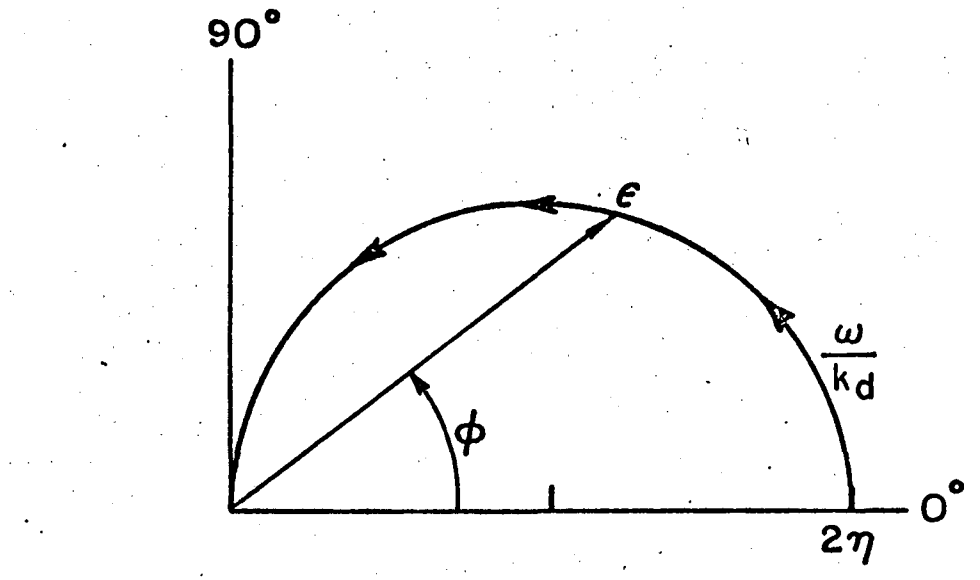

a. Single Process

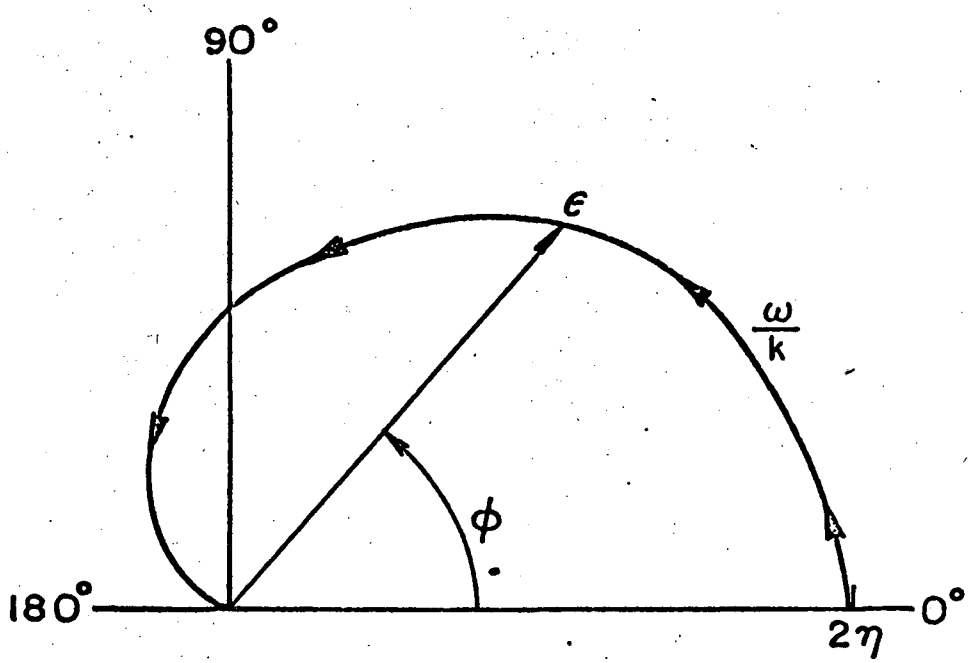

b. Series Process

$k_d = k_1 = k$

XBL717-6986

Fig. 7. Polar plots of the reaction product vector for simple adsorption-desorption and the series process.

TECHNICAL INFORMATION DIVISION
LAWRENCE BERKELEY LABORATORY
UNIVERSITY OF CALIFORNIA
BERKELEY, CALIFORNIA 94720